Supplementary Information for 'Calcium-triggered fusion of lipid membranes is enabled by amphiphilic nanoparticles'

Mukarram A. Tahir[1], Berta Tinao[2], Zekiye P. Guven[3], Yu-Sang Sabrina Yang[4], Alisha N. Bhanji[1], Ahmet Bekdemir[3], Jacob T. Martin[4], Darrell Irvine[1,4], Francesco Stellacci[3], Laura R. Arriaga[2,*], Alfredo Alexander-Katz[1,*]

[1]*Department of Materials Science and Engineering, Massachusetts Institute of Technology, Cambridge, Massachusetts, USA*

[2] *Department of Theoretical Condensed Matter Physics, Autonoma University of Madrid, 28049, Madrid*

[3] *Institute of Materials, Ecole Polytechnique Federale de Lausanne, 1015 Lausanne, Switzerland*

[4]*Koch Institute for Integrative Cancer Research, Massachusetts Institute of Technology, Cambridge, Massachusetts, USA*

* Correspondence should be addressed to: lrarriaga@quim.ucm.es, aalexand@mit.edu

Supplementary Information

Methods

Force field parameterization

The nanoparticle and lipid membranes were parameterized using the Martini 2.1 force field [S1]. The gold core was modeled at an atomistic resolution, with constituent particles organized as a spherical shell interconnected with a fixed bond network and assigned neutral charge. These modeling simplifications were imposed under the assumption that the interaction of the nanoparticle with its environment is primarily governed by the chemistry of surface ligands rather than characteristics of the gold core [S2]. The surface chemistries considered in this work are 1:1 mixtures of 11-mercapto-1-undecanesulphonate (MUS) as the hydrophilic ligand and either of 1-octanethiol (OT) or 1-hexadecanethiol (HDT) as the hydrophobic ligand. Consistent with previous work, the mixture is grafted onto the nanoparticle surface in a checkerboard pattern with a density of 4.62 ligands-nm^{-2}. The ligands are parameterized using standard Martini particle types as shown in Figure S1, and bonded parameters are chosen to be commensurate with previous work with the intent of reproducing nanoparticle structure [S2] and nanoparticle-membrane interactions [S3] as observed in atomistic molecular dynamics simulations. In particular, modeling all bonds with an equilibrium distance of 0.47 nm and harmonic constant of 1250 kJ mol^{-1} and all angles by an equilibrium value of 180 degrees and harmonic constant of 25 kJ mol^{-1} results in good agreement of the nanoparticles' radial distribution functions with atomistic simulations, as shown in Figure S1, and has been demonstrated in previous work to reproduce the lipid tail protrusion mediated pathway of nanoparticle insertion into lipid membranes [S4].

Simulation systems

Initial configurations for 1,2-dioleoyl-sn-glycero-3-phosphocholine (DOPC) lipid bilayers and vesicles were generated using the computational lipidomics scripts of the Martini force field [S5]. The lipid bilayers had minimum lateral dimensions of 15 nm, which was sufficient to ensure that membrane deformations induced by an embedded nanoparticle decayed before reaching the simulation box edge. Vesicles had an approximate diameter of 20 nm, approaching the lower end of synaptic vesicle size distribution [S6], but necessary for maintaining computational tractability of the simulations. Lipid bilayers were equilibrated for a minimum of 300 ns and lipid vesicles were equilibrated for a minimum of 1000 ns. Nanoparticles were incorporated into the lipid membranes using a ramped soft-core van der Waals potential [S7]. Excess anionic charge from the nanoparticle was neutralized by adding sodium counterions to the system. Double bilayer systems (Figure S2) were constructed by stacking pre-equilibrated bilayers and removing intervening solvent to achieve a net inner hydration of approximately 10 water molecules per lipid. Double vesicle systems (Figure S3) were constructed so that the initial head-group separation between the vesicles was approximately 2 nm. Electrostatic condensation of outer membrane leaflets upon influx of Ca^{2+} following stalk formation was simulated through the removal of a subset of *cis* leaflet lipids, consistent with previous simulation studies on the expansion of the fusion stalk during synaptic vesicle fusion [S8].

Simulation parameters

Molecular dynamics simulations were performed using version 4.6.1 of the Gromacs package [S9]. For all simulations, we used leapfrog integration with a timestep of 20 fs. Solvent was explicitly modeled in the simulations using the standard Martini water model. For all simulations, a velocity re-scaling thermostat with a time constant of 1 ps was used for enforcing a constant temperature of 310 K. Pressure coupling was used for maintaining a constant pressure of 1 bar. Semi-isotropic coupling was used for lipid bilayer simulations and isotropic pressure coupling was used for vesicle simulations. Initial equilibration was performed using a Berendsen barostat with coupling time of 3 ps and compressibility of 4.5 x 10^{-5} bar^{-1}. Subsequent equilibration and production runs were performed using a Parrinello-Rahman barostat with coupling time of 1 ps and compressibility of 4.5 x 10^{-5} bar^{-1}. Electrostatic interactions

were shifted to zero between 0 nm and 1.2 nm and screened with a relative permittivity of 15. van der Waals interactions were shifted to zero between 0.9 nm and 1.2 nm. Neighbor lists were updated every 10 steps with a cutoff of 1.4 nm. These parameters were all chosen to be consistent with standard recommendations for the Martini force field.

Transition state analysis

We used committor analysis to identify the transition state for nanoparticle-induced stalk formation between lipid membranes. Committor analysis can uncover transition states without pre-conception of a reaction coordinate, and has previously been used with success to identify transition states of related processes such as membrane fusion [S10]. Simulation frames at 30 ps increments were extracted from a 20 ns interval surrounding the incidence of stalk formation. For each frame, 20 independent simulations lasting for 5 ns each were performed with random initial velocities. The committor, p, was then defined as the probability that the trajectory proceeded towards stalk nucleation (indicated by presence of hydrophobic contact between nanoparticle and adjacent bilayer) or reverted to a separated state (absence of hydrophobic contact). The transition state corresponded to the configuration that was equally likely ($p = 0.5$) to form a stalk or revert to a separated state.

Nanoparticle synthesis and liposome formation

Nanoparticles were synthesized following the Brust method in which the reduction of 0.45 mmol tetrachloroaurate ($HAuCl_4.3H_2O$, Sigma Aldrich) takes place with the presence of thiols (0.225 mmol mercaptoundecano sulfonate $C_{11}H_{23}O_3S$, synthesized in the lab and 0.225 mmol octanethiol $C_8H_{18}S$, Sigma Aldrich) by 13 mmol sodium borohydride ($NaBH_4$, Sigma Aldrich) in ethanol at room temperature [S11]. All 1,2-dioleoyl-sn-glycero-3-phosphocholine (DOPC, $C_{44}H_{84}NO_8P$, Avanti Lipids) vesicles were prepared by lipid film hydration as 5mM hydrated lipid mixture was extruded with 200 nm, 100 nm, 50nm, and 30 nm filters, successively.

Experimental conditions

For cryogenic imaging, 2.5 mM of vesicles were incubated with a final concentration of 0.1 mg/ml nanoparticles of 1:1 MUS:OT surface chemistry (30% OT by NMR SX, 2.4 ± 1.7 nm of core size) at final volume of 30 µl at room temperature for 1 hour without any agitation. To initiate fusion, $CaCl_2$ solution was added from a concentrated 100 mM solution to final 2 mM concentration. Cryo samples of systems containing $CaCl_2$ were prepared directly after addition of $CaCl_2$.

Cryogenic transmission electron microscopy

Grids for tomograms were prepared in a commercial vitrification system (Vitrobot Mark IV, FEI, Netherlands) with 100% humidity at 22˚C. 4 µl of sample was pipetted on a lacey carbon grid (300 mesh, Electron Microscopy Science, Hatfield, PA) which was glow discharged for 3 seconds beforehand. Prior to plunge freezing, excess sample was blotted with blotting force of -15 for 2 seconds. After plunge freezing, the grids were transferred at -178˚C into a Gatan 626 cryo-holder (Gatan Inc. Warrendale, PA.) and imaged in a FEI Tecnai F20 microscope (FEI) operated at 200kV. Total electron dose for one image was between 25-35 e/Å^2 and was acquired using magnifications of 50000X and 62000X (pixel size 0.2 nm and 0.16 nm respectively) with defocus value of -2.4 µm. Images were recorded by a BM-Ceta camera (4096 x 4096 pixels, FEI)

Electroformation of GUVs

DOPC and DOPE-Rho stock solutions (10 and 1 mg/mL, respectively) were prepared in chloroform. Appropriate volumes of these stocks were mixed to yield a final DOPC solution of 0.5 mg/mL labeled with 0.5 mol.% of DOPE-Rh. Then, approximately 10 µL of this solution (three drops) was deposited on the surface of an ITO surface. After evaporation of the chloroform, a chamber was built around the dry lipid material using a water-resistant putty. A

second ITO surface with the same lipid deposit was placed on top of the putty in a sandwich configuration. The chamber was then filled with a 200 mM sucrose solution (the capacity of the chamber was approximately 400 μL) to hydrate the dry lipid material. An electrode made of copper tape was placed on each of the ITO conductors, and connected to a computer. Using Audacity, we applied a sinusoidal current (10 Hz, ~ 1 V) for 2h at room temperature.

GUV production by microfluidics

Giant unilamellar vesicles (GUVs) were formed using water-in-oil-in-water double emulsion drops with ultrathin oil shells as templates [S12]. To produce these templates, we used a glass-capillary device that consisted of two round capillaries, a hydrophobic injection capillary on the left, and a hydrophilic collection capillary on the right, both inserted into a square capillary and axially aligned under a microscope, as illustrated schematically in Figure S10A. An innermost aqueous phase containing 9 wt% dextran (70 kDa, Sigma) and 1 wt% polyvinyl alcohol (PVA, 13-23 kDa, 87% hydrolyzed, Sigma) was injected in the device through an additional smaller capillary inserted into the left injection capillary. A middle oil phase consisting of 5 mg/mL DOPC (Avanti Lipids) dissolved in a mixture of 36% chloroform and 64% hexane was then injected through the left injection capillary. An outer aqueous phase containing 10 wt% PVA was finally injected in the device through the interstices between the square capillary and the left injection capillary. Using this configuration, double emulsions with ultrathin oil shells were formed at the tip of the injection capillary in the discontinuous dripping regime [S13], and pulled further downstream into the collection capillary by the outer aqueous phase, as shown in the optical microscope image of Figure S10B and Supplementary Movie S6. These double emulsions were collected in a large excess of milli-Q water. Dewetting of the middle phase solvents from the double emulsions resulted in the formation of GUVs [S12]. These GUVs were then used for the GUV-liposome fusion assays shown in the Supplementary Movies S4-S5.

Fusion assays

Fluorometer assays:

Content mixing: To form liposomes containing sulforhodamine B at self-quenching concentration, 80 μl of 10 mg/ml of 1,2-dioleoyl-sn-glycero-3-phosphocholine (DOPC, $C_{44}H_{84}NO_8P$, Avanti Lipids) solution in chloroform was first dried in a dessicator. Then 200 μl of 50 mM sulforhodamine B ($C_{27}H_{30}N_2O_7S_2$, Sigma Aldrich) in 2.5 mM Tris was added to the dried lipid film and sonicated at 50˚C for 2 hours. Free ligands were cleaned by three rounds of centrifugation at 100,000 G for 50 minutes each. The pellet was slowly dispersed with 2.5 mM Tris and 50 mM NaCl buffer to a 2 mg/ml final concentration. To conduct the content mixing experiments on liposomes, liposomes containing sulforhodamine B were mixed at a 1:1 ratio with free liposomes and nanoparticles, and incubated following cryo conditions for 1 hour. Calcium was introduced to the samples slowly having a final concentration of 2 mM. The fluorescent measurements were done on the samples that were 40 times diluted to avoid saturation of the signal.

Lipid mixing: A stock solution of 1,2-dioleoyl-sn-glycero-3-phosphocholine (DOPC, Avanti Polar Lipids, solid powder) is prepared by dissolving DOPC in chloroform to a final concentration of 100 mg/mL. 1,2-dipalmitoyl-sn-glycero-3-phosphoethanolamine-N-(7-nitro-2-1,3-benzoxadiazol-4-yl) (ammonium salt) (DPPE-NBD) and 1,2-dipalmitoyl-sn-glycero-3-phosphoethanolamine-N-(lissamine rhodamine B sulfonyl) (ammonium salt) (DPPE-Rh) are purchased from Avanti Polar Lipids as chloroform solutions at a concentration of 1 mg/mL each. Appropriate volumes of unlabeled DOPC and labeled DPPE stock solutions are mixed to yield a ratio of 99.5 mol% unlabeled DOPC and 0.5 mol.% labeled DPPE and a total lipid mass of 10 mg after chloroform evaporation. The resultant dried lipid films are hydrated with 1 mL of milli-Q water at room temperature for one hour. During hydration, the suspension is frequently vortex. After hydration, the suspension is extruded 21 times through a polycarbonate membrane with a nominal pore size of 100 nm using a extruder (mini-extruder, Avanti); this yields large unilamellar vesicles (LUVs). This approach is used to prepare two different populations of LUVs, one labeled with DPPE-NBD, referred as NBD-LUVs, which act as donors, and the other one labeled with DPPE-Rh, referred as Rh-LUVs, which act as acceptors. Equal volumes of the two populations of LUVs are mixed to yield a total lipid concentration of 2.5 mg/mL in a 50 μL total volume for all the samples prepared. NPs are added from a stock solution of 2 mg/mL to a final concentration of 0.1 mg/mL and incubated with the LUVs for at least 30 min before measurement or Ca^{2+} addition. Ca^{2+} is added from a stock solution of 10 mM to a final concentration of 2 mM and incubated with LUVs for at least 30 min before measurement

or quencher addition. As a quencher for NBD fluorescence, we use sodium-dithionite, which is added to the sample from a stock solution of 250 mM to a final concentration of 50 mM. For FRET measurements, the different 50 μL samples prepared are poured into a 50 μL quartz cuvette. The emission spectrum of the mixture of NBD-LUVs and Rh-LUVs in different conditions is then measured at an excitation wavelength of 463 nm, which is the excitation wavelength of the donor (NBD) in a spectrofluorometer AMINCO Bowman Series 2 (Spectronic Instruments, Model FA257) with a 60% of laser power, a detector voltage of 600 V, and a step size of 1 nm.

Confocal microscopy assays: 25 μl of electroformed DOPC GUVs labeled with DOPE-Rho where mixed with 25 μl of SUVs labeled with DOPE-NBD containing 50 mM sulforhodamine B. The mixture was incubated for 30 min. The chamber was sealed during this incubation period with a second cover slip to avoid evaporation. $CaCl_2$ was added to the sample from a 100 mM stock solution to a final concentration of 2 mM in the observation chamber. A second aliquot (25 μl) of these SUVs was incubated with 1.5 μl of MUS:OT nanoparticles (2 mg/ml) on a second chamber. This aliquot was mixed with 25 μl of electroformed DOPC GUVs labeled with DOPE-Rho and incubated for 30 min. The same procedure described above was used to add $CaCl_2$ to this sample. Samples were visualized by confocal fluorescence microscopy (Nikon Eclipse Ti, 40x water immersion objective) using two different lasers with excitation wavelengths of 480 and 561 nm, respectively. The first laser excites DOPE-NBD in the membrane of the SUVs, whereas the second laser excites DOPE-Rho in the membrane of the GUVs and the sulforhodamine B molecules in the inner cores of the SUVs. Using this configuration, the inner cores of GUVs should become red upon fusion of SUVs with GUVs. FRET was performed on the same confocal microscope using a single laser. DOPE-NBD was excited with the 480 nm laser, whereas the 561 nm laser was turned off. Using this configuration, DOPE-Rho should become visible when its distance to DOPE-NBD molecules is smaller than 10 nm.

To conduct the content mixing experiments on GUVs formed by microfluidics, 1 μL of MUS:OT nanoparticles, 10 μL of liposomes containing sulforhodamine B at self-quenching concentration and 200 μL of GUVs were added within a microscope chamber. This system was incubated for 1 h and monitored by fluorescence confocal microscopy during incubation. No fusion was observed during this incubation period. Following incubation, an aliquot of Ca^{2+} was added slowly into the chamber from a 20 mM $CaCl_2$ solution to a final concentration of 10 mM. Fusion between liposomes and GUVs was then visualized by fluorescence confocal microscopy (Nikon Eclipse Ti) using a 10 dry objective, an excitation wavelength of 561 nm and a band pass filter between 570 and 1000 nm to collect the emission.

Supplementary References

[S1] Marrink, S. J., Risselada, H. J., Yefimov, S., Tieleman, D. P., & De Vries, A. H. (2007). The MARTINI force field: coarse grained model for biomolecular simulations. *The Journal of Physical Chemistry B*, 111(27), 7812-7824.

[S2] Van Lehn, R. C., & Alexander-Katz, A. (2013). Structure of mixed-monolayer-protected nanoparticles in aqueous salt solution from atomistic molecular dynamics simulations. *The Journal of Physical Chemistry C*, 117(39), 20104-20115.

[S3] Van Lehn, R. C., Atukorale, P. U., Carney, R. P., Yang, Y. S., Stellacci, F., Irvine, D. J., & Alexander-Katz, A. (2013). Effect of particle diameter and surface composition on the spontaneous fusion of monolayer-protected gold nanoparticles with lipid bilayers. *Nano letters*, 13(9), 4060-4067.

[S4] Simonelli, F., Bochicchio, D., Ferrando, R., & Rossi, G. (2015). Monolayer-protected anionic Au nanoparticles walk into lipid membranes step by step. *The Journal of Physical Chemistry Letters*, 6(16), 3175-3179.

[S5] Wassenaar, T. A., Ingólfsson, H. I., Böckmann, R. A., Tieleman, D. P., & Marrink, S. J. (2015). Computational lipidomics with insane: a versatile tool for generating custom membranes for molecular simulations. Journal of chemical theory and computation, 11(5), 2144-2155.

[S6] Zhang, B., Koh, Y. H., Beckstead, R. B., Budnik, V., Ganetzky, B., & Bellen, H. J. (1998). Synaptic vesicle size and number are regulated by a clathrin adaptor protein required for endocytosis. *Neuron*, 21(6), 1465-1475.

[S7] Jefferys, E., Sands, Z. A., Shi, J., Sansom, M. S., & Fowler, P. W. (2015). Alchembed: a computational method for incorporating multiple proteins into complex lipid geometries. *Journal of Chemical Theory and Computation*, 11(6), 2743-2754.

[S8] Risselada, H. J., Bubnis, G., & Grubmüller, H. (2014). Expansion of the fusion stalk and its implication for biological membrane fusion. *Proceedings of the National Academy of Sciences*, 111(30), 11043-11048.

[S9] Hess, B., Kutzner, C., Van Der Spoel, D., & Lindahl, E. (2008). GROMACS 4: algorithms for highly efficient, load-balanced, and scalable molecular simulation. *Journal of Chemical Theory and Computation*, 4(3), 435-447.

[S10] Kasson, P. M., Lindahl, E., & Pande, V. S. (2010). Atomic-resolution simulations predict a transition state for vesicle fusion defined by contact of a few lipid tails. *PLoS Computational Biology*, 6(6), e1000829.

[S11] Verma, A., Uzun, O., Hu, Y., Hu, Y., Han, H. S., Watson, N., Chen, S., Irvine, D. J., & Stellacci, F. (2008). Surface-structure-regulated cell-membrane penetration by monolayer-protected nanoparticles. *Nature Materials*, 7(7), 588.

[S12] Arriaga, L.R., Datta, S.S., Kim, S.-H., Amstad, E., Kodger, T.E., Monroy, F. & Weitz, D.A. (2014). Ultra-thin shell double emulsion template giant unilamellar lipid vesicles with controlled microdomain formation. *Small*, 10(5), 950-956.

[S13] Kim, S.-H, Kim, J.W., Cho, J.C. & Weitz, D.A. (2011). Double-emulsion drops with ultra-thin shells for capsule templates. *Lab on a Chip*, 11(18), 3162-3166.

Supplementary Figures

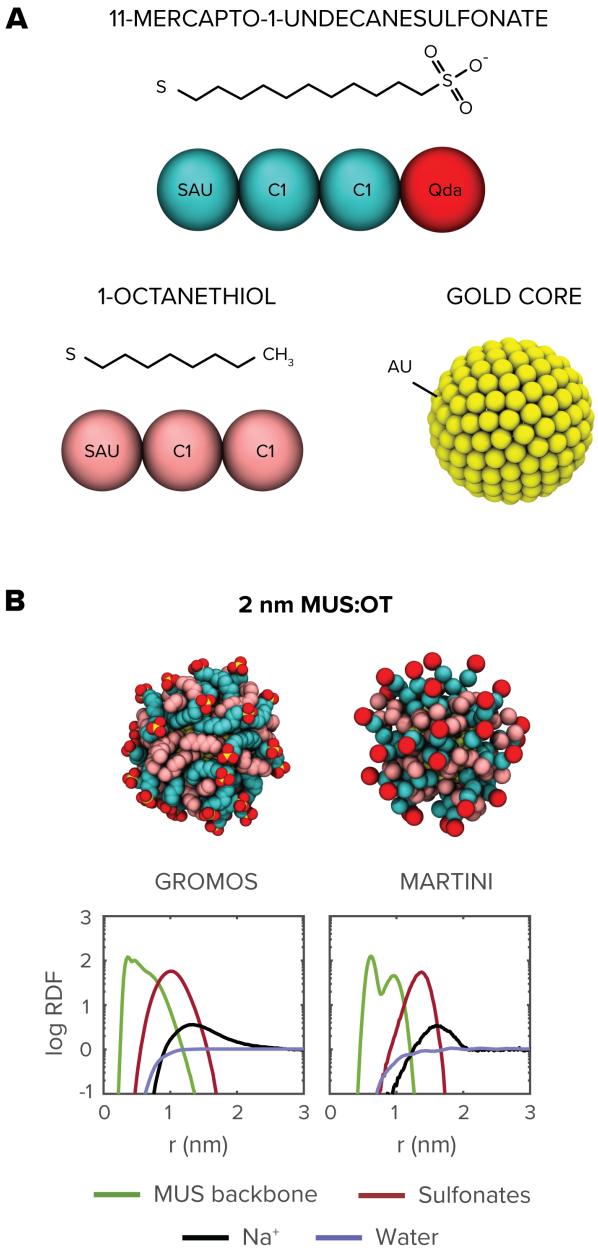

Figure S1 – Computational model of system components. (a) Parameterization of monolayer-protected nanoparticle using the Martini bio-molecular force field. Model parameters and assumptions are discussed in the Supplementary Methods. (b, c) Snapshots and radial distribution functions comparing atomistic and coarse-grained parameterizations of 2 nm MUS:OT nanoparticles.

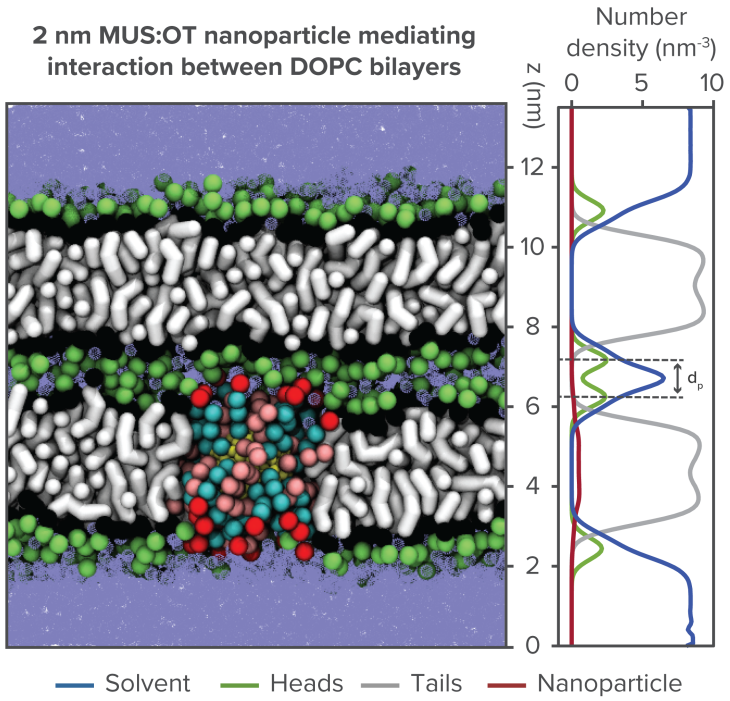

Figure S2 – Quantitative characterization of planar double bilayer system. Explicit-solvent snapshot of DOPC lipid membranes separated by a dehydrated interface containing approximately 10 water molecules per lipid and a single 2 nm MUS:OT nanoparticle embedded in the lower membrane. The dehydration results in an inner head group distance (d_p) of approximately 1 nm. The plot on the right shows the number density of solvent, lipid heads, lipid tails, and nanoparticle time-averaged over initial 10 ns of the production simulation.

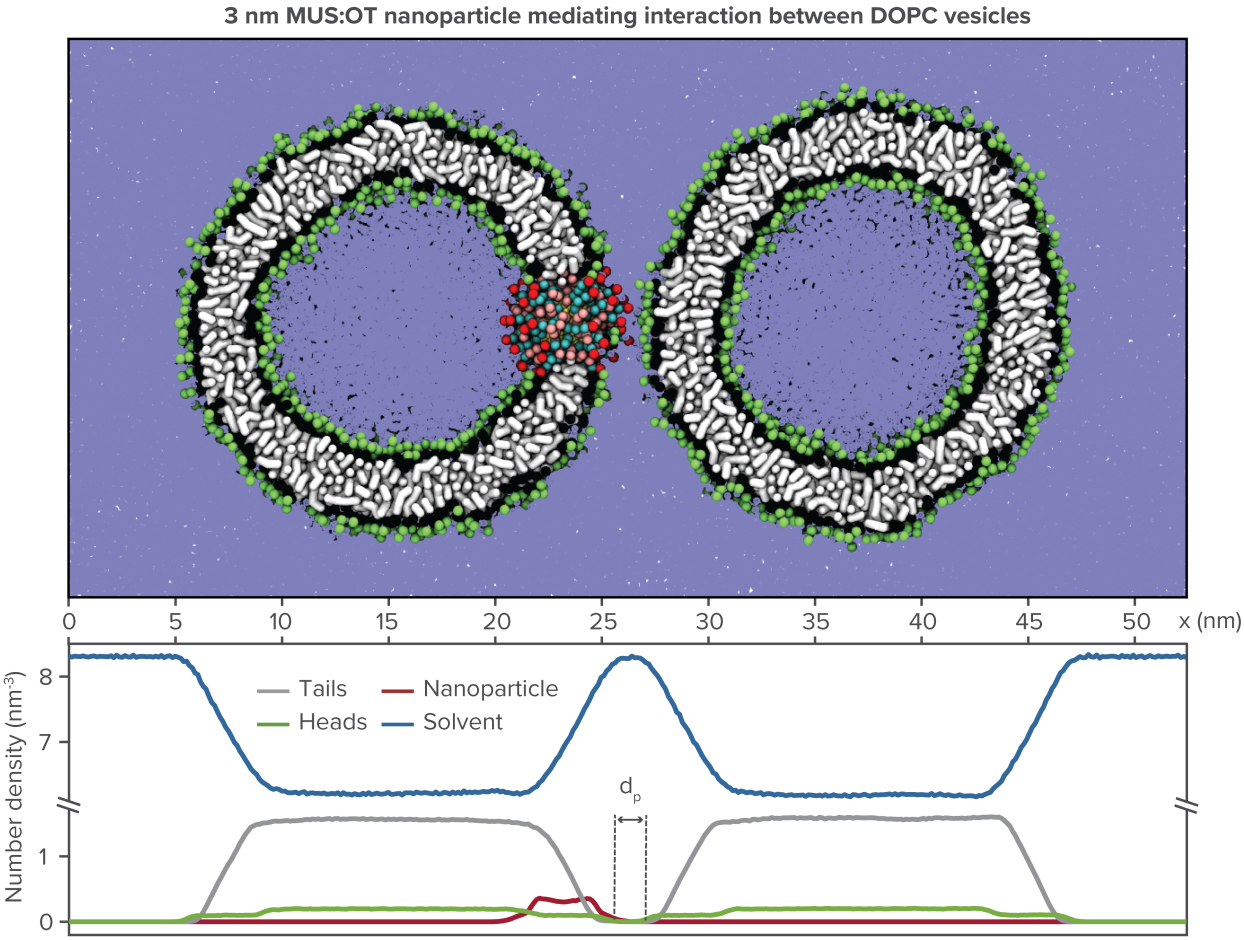

Figure S3 – Quantitative characterization of double vesicle system. Explicit-solvent snapshot of DOPC lipid vesicles, with a single 3 nm MUS:OT nanoparticle embedded in the left vesicle. The vesicles are initially positioned so that the head group separation (d_p) is approximately 2 nm at the start of the simulation. The plot on the bottom shows the number density of solvent, lipid heads, lipid tails, and nanoparticle time-averaged over initial 10 ns of the subsequent simulation.

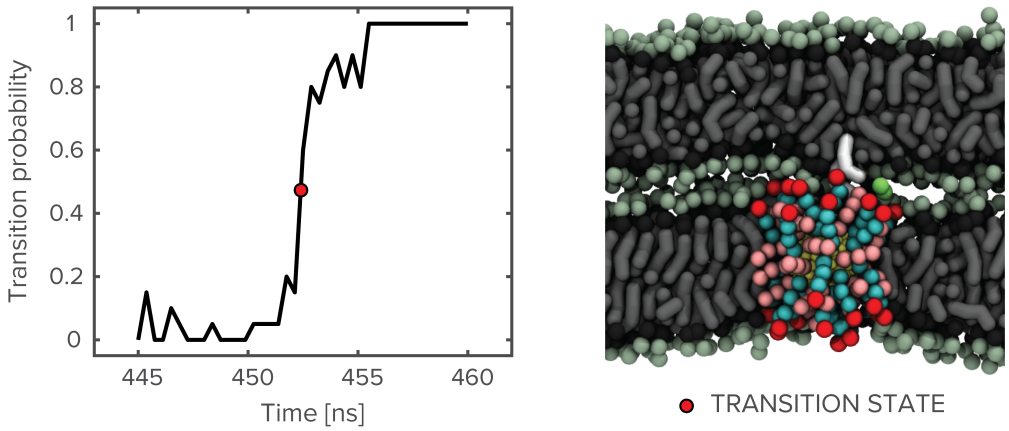

Figure S4 – Committor analysis of nanoparticle-induced stalk formation. Probability of transition to a stalk as estimated from committor analysis of the simulation trajectory containing a 2 nm MUS:OT nanoparticle mediating interaction between planar DOPC lipid membranes. The transition state corresponds to the simulation frame where $p = 0.5$, and consists of the nanoparticle extracting a lipid from the adjacent membrane.

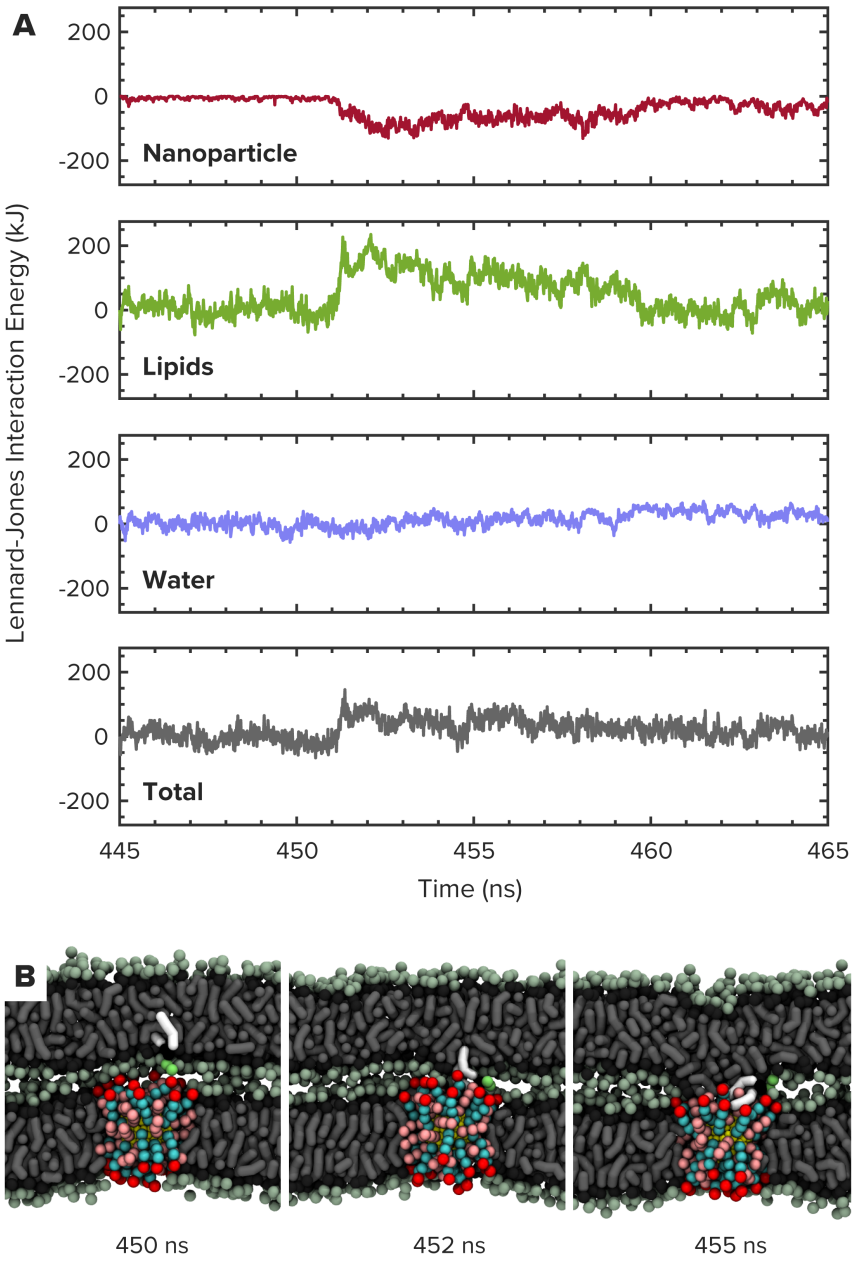

Figure S5 – Analysis of nanoparticle-induced lipid extraction. (a) The Lennard-Jones interaction energy between the (eventually) extracted lipid and system constituents is shown in the vicinity of the transition state. While extraction incurs an energetic penalty from the viewpoint of lipids in the system, favorable interaction with the exposed amphiphilic ligands of the nanoparticle provides a compensating decrease in interaction energy, allowing for lipid extraction within hundreds of nanoseconds. (b) Snapshots from the corresponding simulation highlighting initial lipid extraction and subsequent lipid mixing that contributes to stalk formation between the lipid membranes.

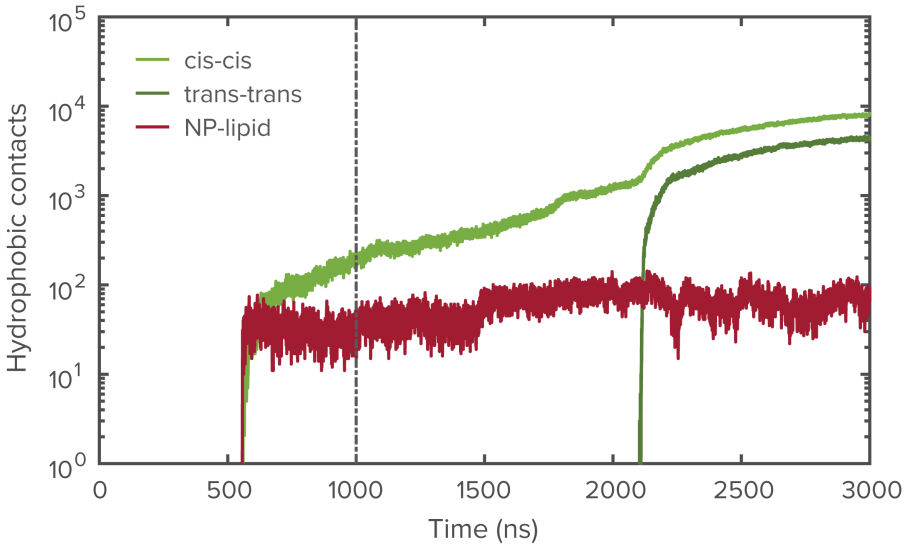

Figure S6 – Quantitative analysis of nanoparticle-mediated vesicle fusion. Time series of the number of hydrophobic contacts between the proximal leaflets of the two vesicles (*cis*-*cis*), between distal leaflets of the two vesicles (*trans*-*trans*), and between nanoparticle ligands and lipids from the adjacent vesicle (NP-lipid) are shown over the course of the initial unbiased simulation (left of the dashed line), and following deletion of a subset of *cis* leaflet lipids from both vesicles (right of the dashed line).

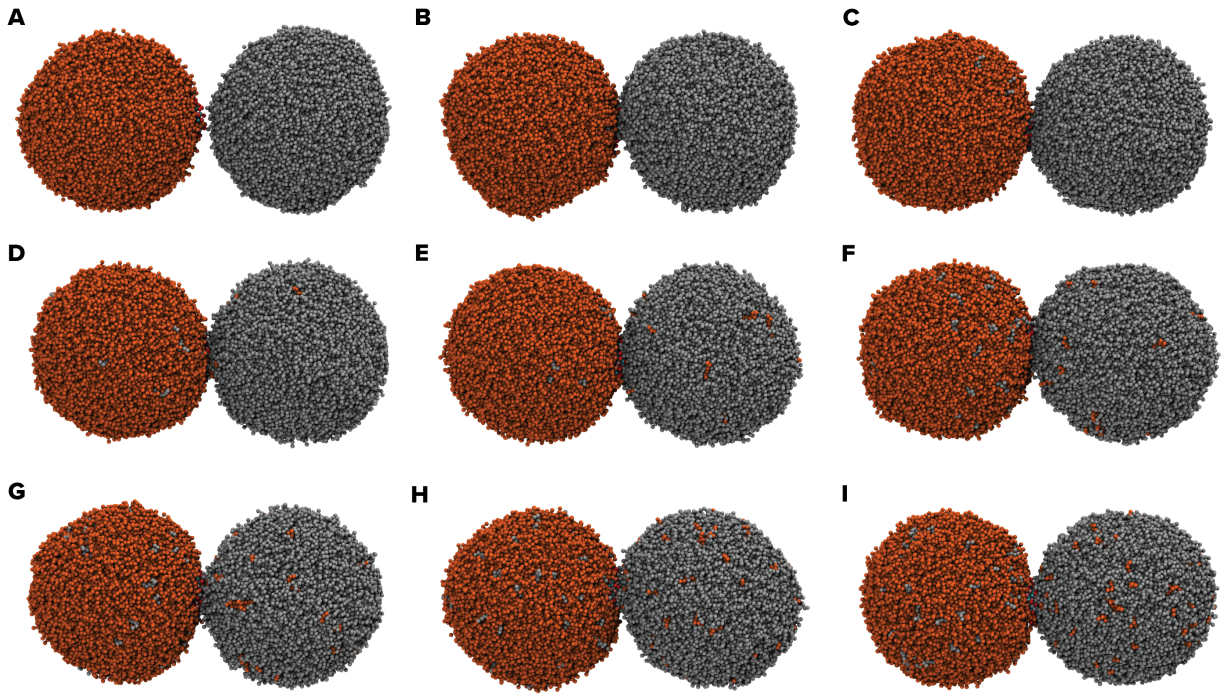

Figure S7 – Outer-leaflet mixing following nanoparticle-induced stalk formation. Snapshots demonstrating *cis* leaflet mixing between vesicles following stalk formation. After initial extraction of a lipid from the adjacent vesicle, the nanoparticle functions as a bridge over which subsequent lipid exchange occurs between outer membrane leaflets. At this stage, no exchange occurs between *trans* leaflets of the two vesicles.

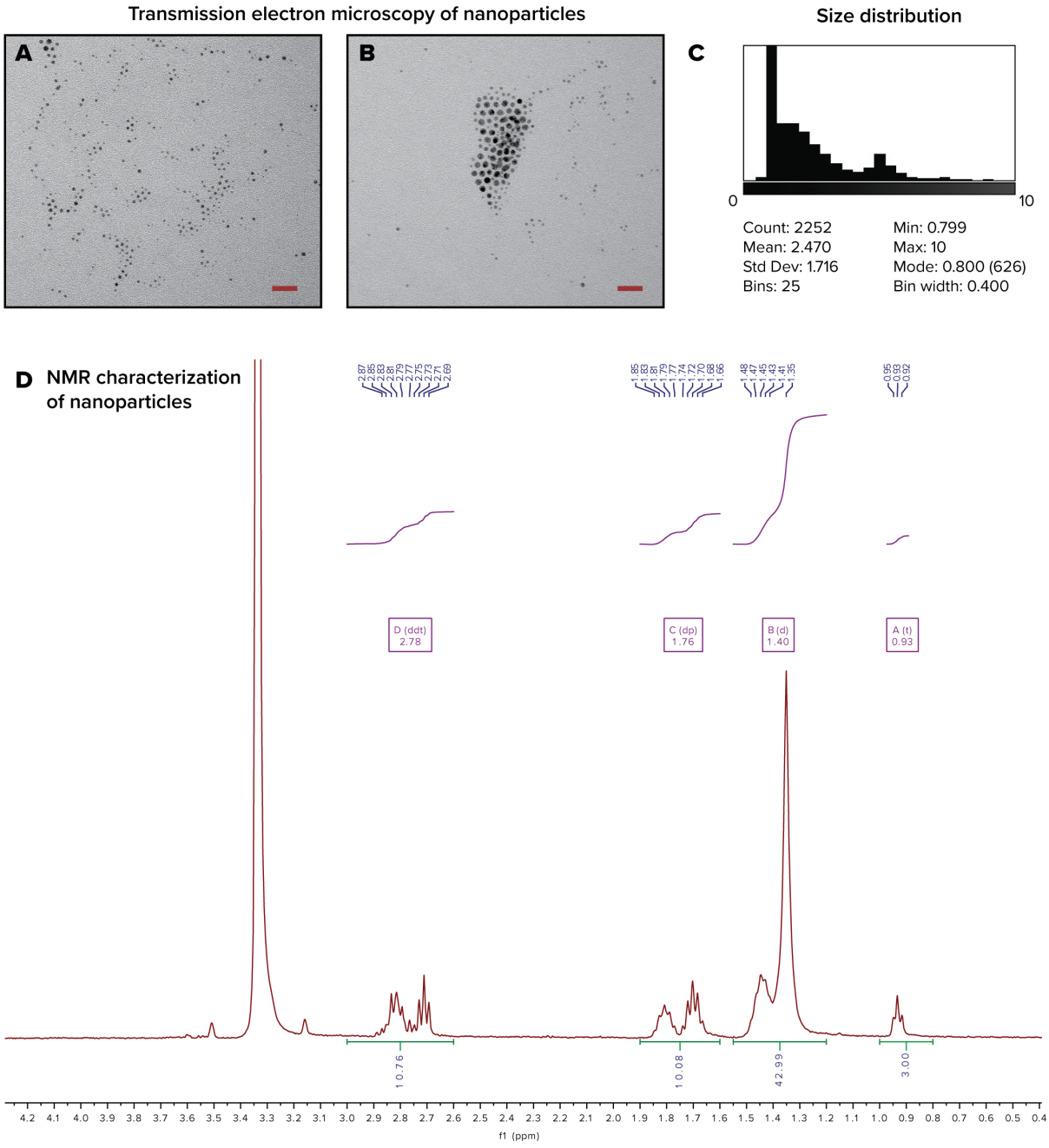

Figure S8 – Characterization of 2:1 MUS:OT nanoparticles. (a) Transmission electron microscopy images of nanoparticles. (b) Size distribution of nanoparticle core diameters as obtained from TEM. (c) NMR characterization of the nanoparticle batch.

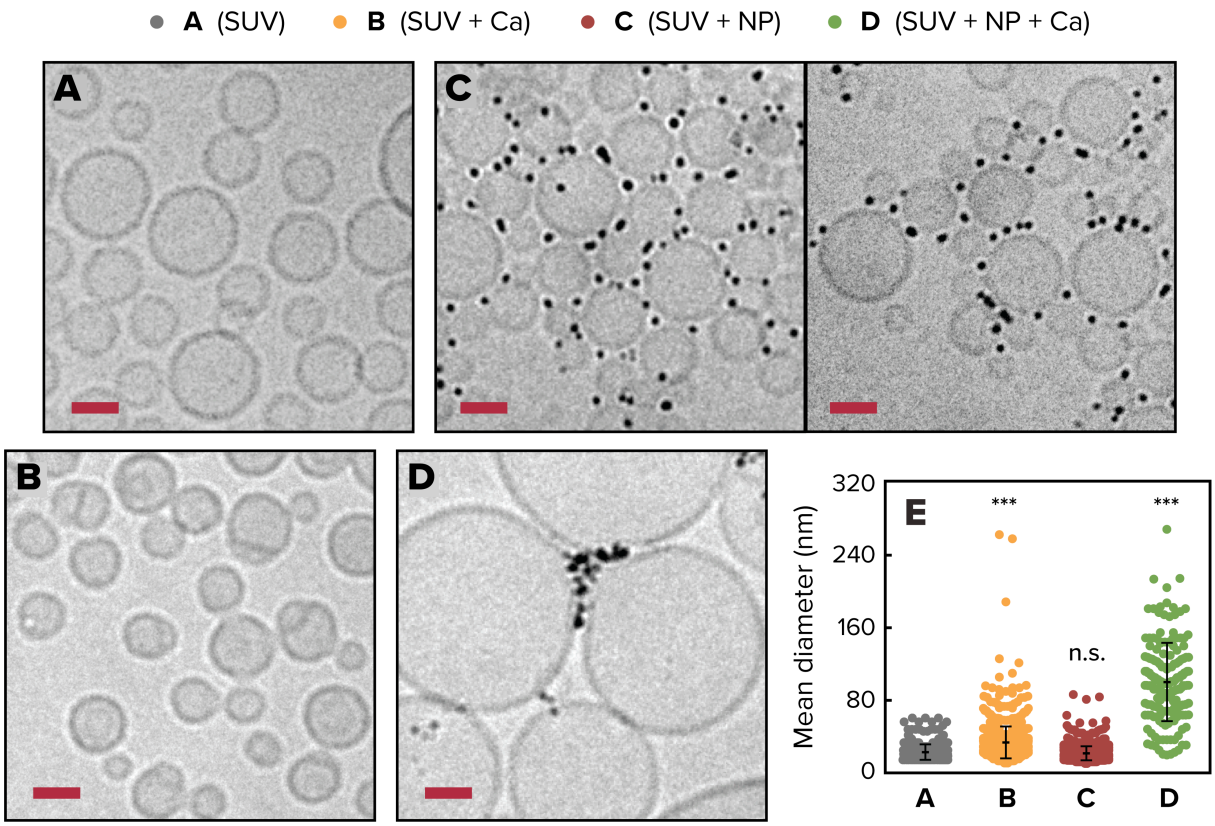

Figure S9 – Cryogenic transmission electron microscopy of vesicle fusion driven by amphiphilic nanoparticles. Experiments presented in the main text were repeated with higher vesicle and nanoparticle concentrations. (a) Unilamellar DOPC vesicles as synthesized. (b) Vesicles upon addition of $CaCl_2$ in absence of nanoparticles. (c) Vesicles upon addition of 3 nm MUS:OT gold nanoparticles. (d) Vesicles upon influx of $CaCl_2$ following incubation with nanoparticles. (e) Size distribution of liposomes corresponding to these conditions as determined from quantitative analysis of the microscopy images. Scale bars are 25 nm.

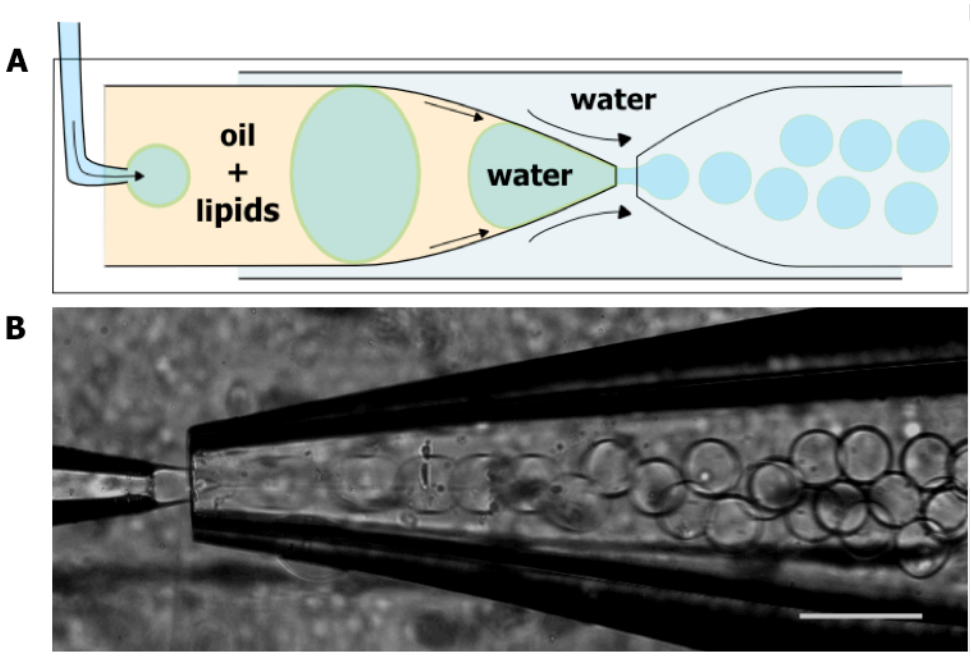

Figure S10 – Formation of giant unilamellar vesicles using microfluidics. a) Schematic illustration of the glass-capillary device used to produce double emulsion templates. b) Optical microscope image showing a typical production. Scale bar is 200 μm.

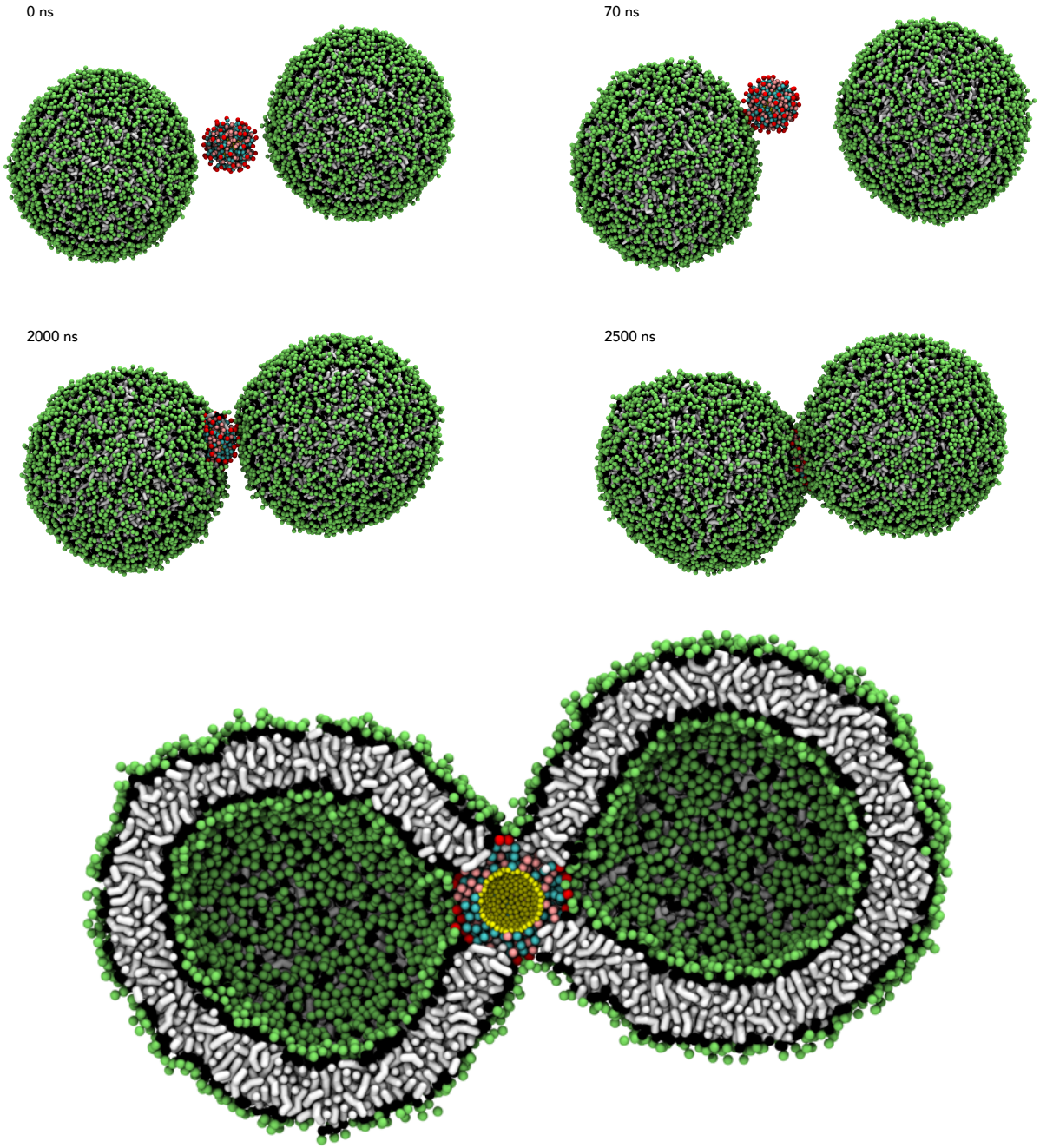

Figure S11 – Molecular dynamics simulation of free nanoparticle-driven stalk formation. Coarse-grained molecular dynamics simulations in the presence of a free nanoparticle between 2 vesicles. After approximately 2μs the particle has hemifused with both vesicles forming a symmetric stalk (lower panel) reminiscent of the ones seen in the cryo-TEM pictures.

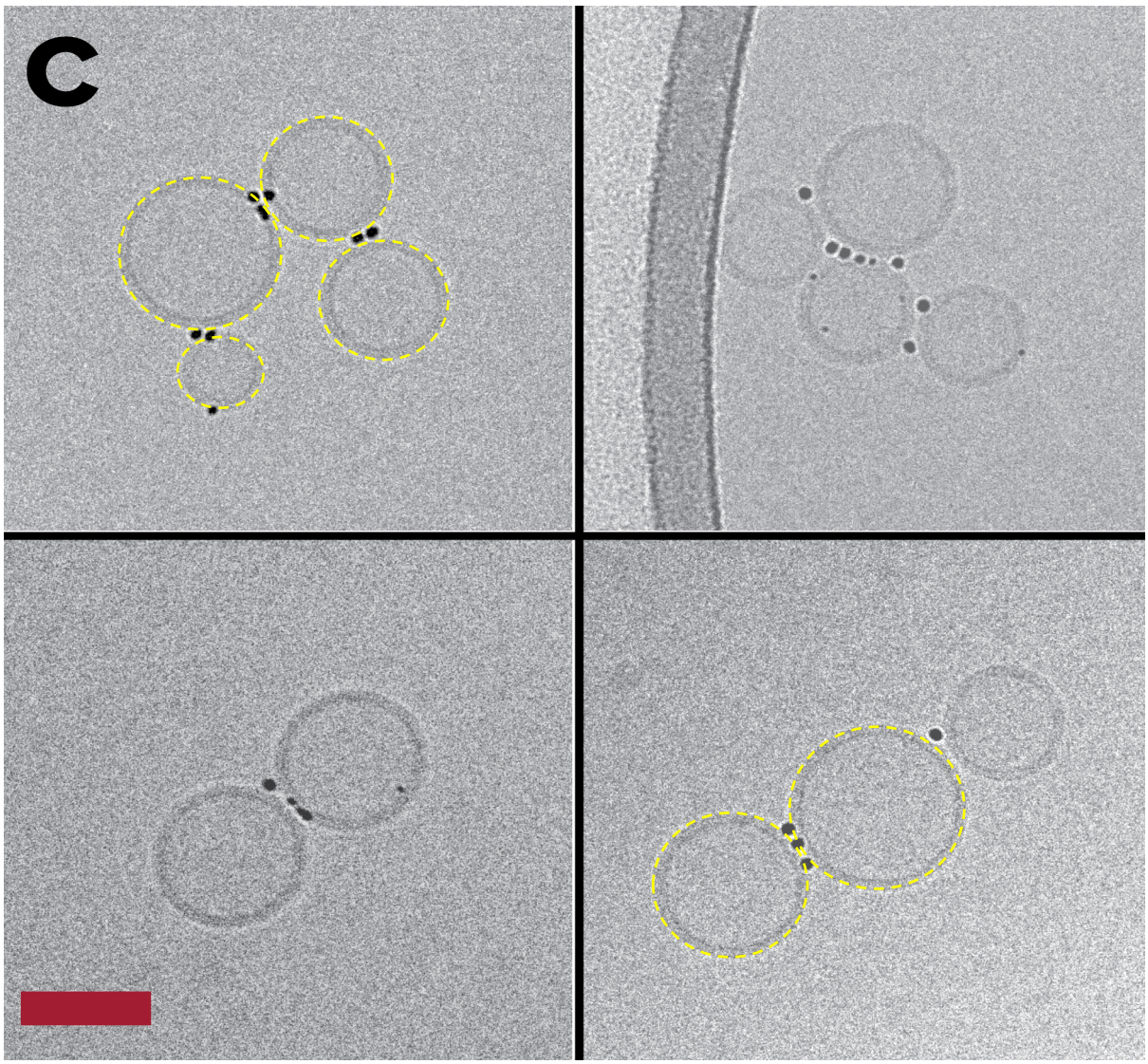

Figure S12 – Cryo-TEM of SUVs in presence of NPs. The same snapshots as in Figure 3c in the main text, but with some of the edges of the vesicles drawn in dashed yellow lines to show that the NPs are in contact with the lipid tails.

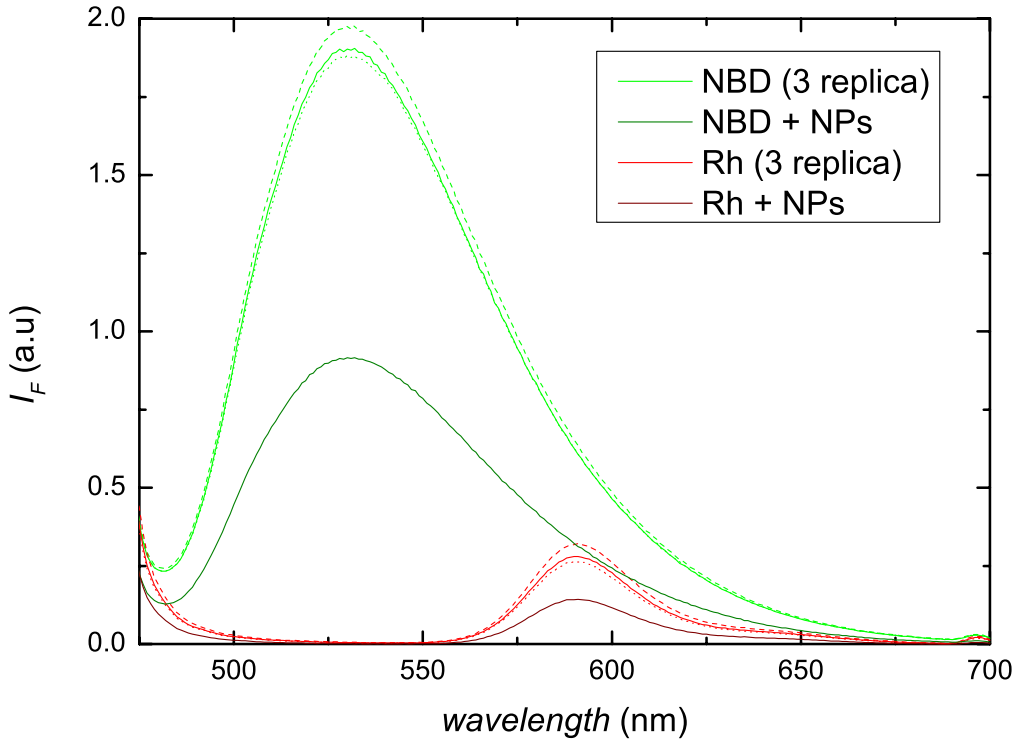

Figure S13 –Spectra of the FRET pair dyes by themselves when excited at 463nm. The NBD-PE has a maximum emission at 536nm and the Rh-PE has a maximum emission at 583nm. Note that while the excitation wavelength for Rh-PE is around 560, it still has a residual adsorption from the excitation at 463nm. We use this results to obtain the actual FRET signal in Fig. 3G by subtracting the Rh-NP signal from this plot. Important to not here is that NPs quench the signal in for both dyes significantly.

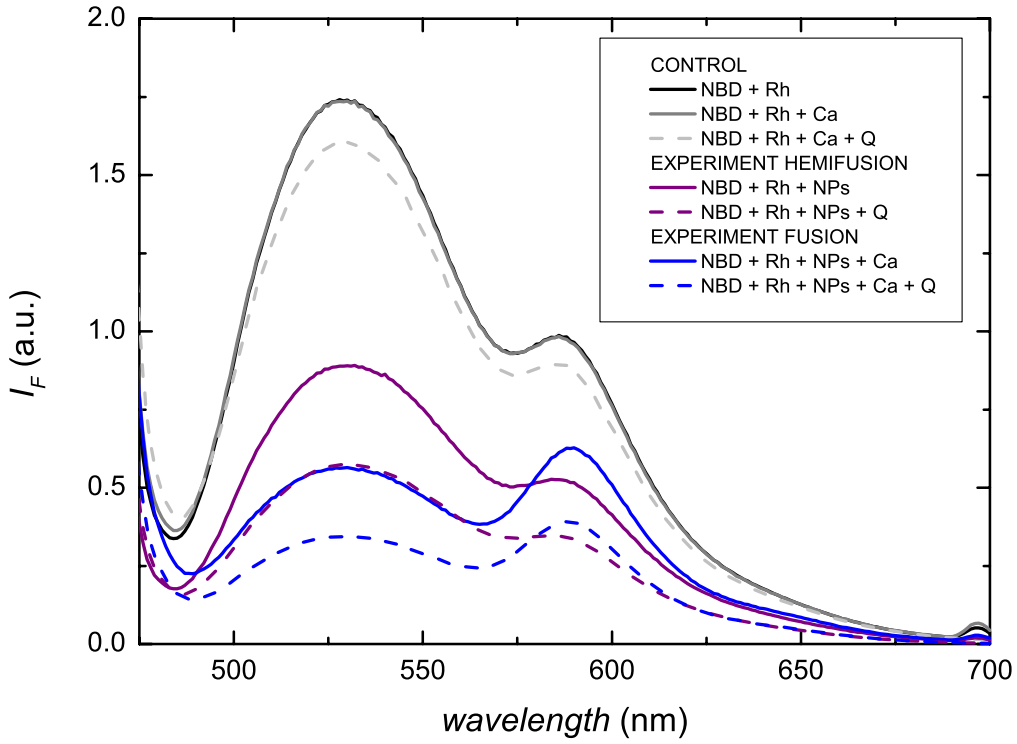

Figure S14 – FRET Spectra before and after quenching. Fluorescence from different conditions as explained in the legend. Q stand for quencher. Fig. 3G is based on this data, except that the background signal from Fig. S13 has been subtracted. Notice the strong FRET signal at 582 nm in the blue curves before and after the quencher has been added implying full fusion. Also note that the NPs quench the signal considerably.

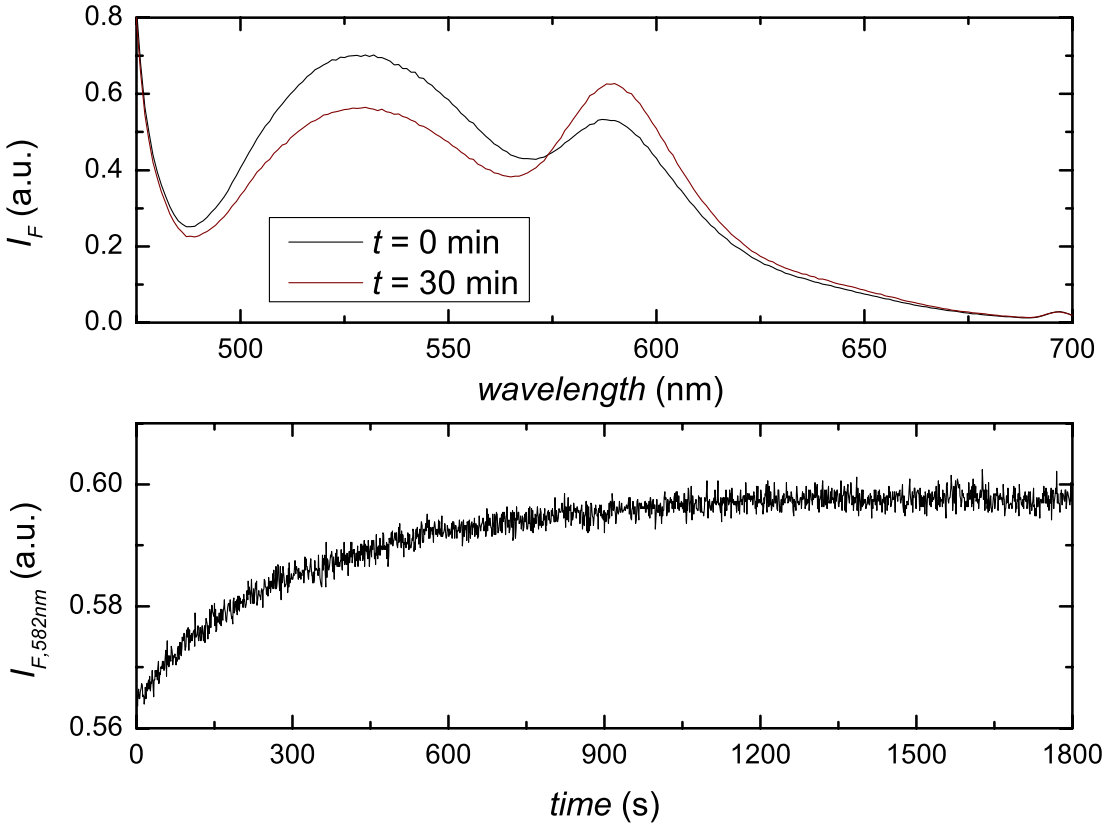

Figure S15 –Time dependent FRET signal after Ca addition. Fluorescence spectra from the NBD-PE and Rh-PE SUV system incubated with MUS:OT after addition of 2mM $CaCl_2$. We observe two regimes, a very fast regime that cannot be captured with the present protocol that occurs within the first seconds upon mixing and a second slower mixing regime that extends up to approximately 20min. The fast mixing can be seen by comparing the black curve with the NPs only curve in Fig. S14. Notice the rapid appearance of a larger peak at 582nm.

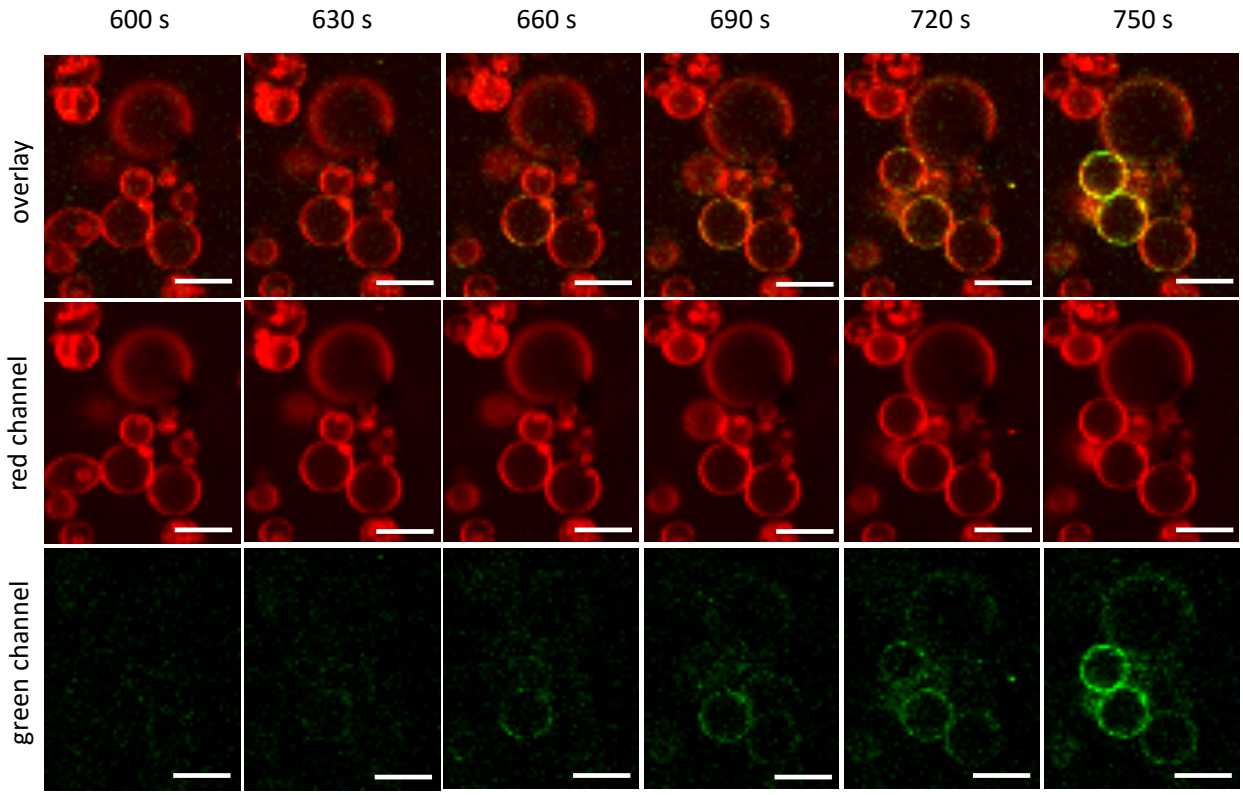

Figure S16 –Time trajectory of lipid mixing in GUVs. The sample of GUVs + SUVs + NPs is incubated with $CaCl_2$ and for this particular set of vesicles we observe rapid lipid mixing (within 10s of seconds) after a lag time of ~600 s. The GUVs were labeled with Sulforhodamine B (red) and the SUVs were labeled with NBD (green). Scale bar is 50μm.

Supplementary Movies

Movie S1 – Nanoparticle-induced stalk formation between planar lipid membranes, as observed in coarse-grained molecular dynamics simulations. Following a latent period, hydrophobic contact between the nanoparticle and lipids from the adjacent bilayer results in the formation of a toroidal stalk that subsequently allows sustained lipid mixing between the proximal leaflets of the two bilayers.

Movie S2 – The transition state for stalk formation is the extraction of a lipid from the adjacent bilayer towards the nanoparticle. In the vicinity of the transition state (~452 ns), plots of the interaction energy between this extracted lipid and system constituents reveal that the energetic penalty for lipid extraction is significantly compensated by association of the lipid with the exposed amphiphilic monolayer of the nanoparticle.

Movie S3 – Coarse-grained molecular dynamics simulations reveal a mechanism through which nanoparticles can drive fusion between lipid membranes. The presence of a membrane-embedded nanoparticles drives the vesicles into close proximity, which in turn facilitates the ability of the nanoparticle to extract lipids from the apposing bilayer and nucleate the formation of a fusion stalk between the membranes. Subsequent influx of Ca^{2+} results in mechanical tension between the inner and outer leaflets of this complex, modeled here by removed of a subset of lipids from the outer leaflets of the vesicles as explained in the text, and this causes expansion of the stalk into a fusion pore.

Movie S4 – Fusion between liposomes containing sulforhodamine B at self-quenching concentration and an empty GUV in the presence of nanoparticles upon addition of Ca^{2+}. A time sequence comprising 100 frames was taken every 10 s after addition of Ca^{2+}. The movie is accelerated 250 times.

Movie S5 – Absence of fusion between liposomes containing sulforhodamine B at self-quenching concentration and empty GUVs in the absence of nanoparticles upon addition of Ca^{2+}. A time sequence comprising 190 frames was taken every 10 s after addition of Ca^{2+}. The movie is accelerated 250 times.

Movie S6 – Production of double emulsion drops with ultrathin shells. The movie is slowed down by a factor of 40 for visualization. Typical production rate is 300 emulsion/s.